One Earth

Article

Alternative-energy-vehicles deployment delivers climate, air quality, and health co-benefits when coupled with decarbonizing power generation in China

Graphical abstract

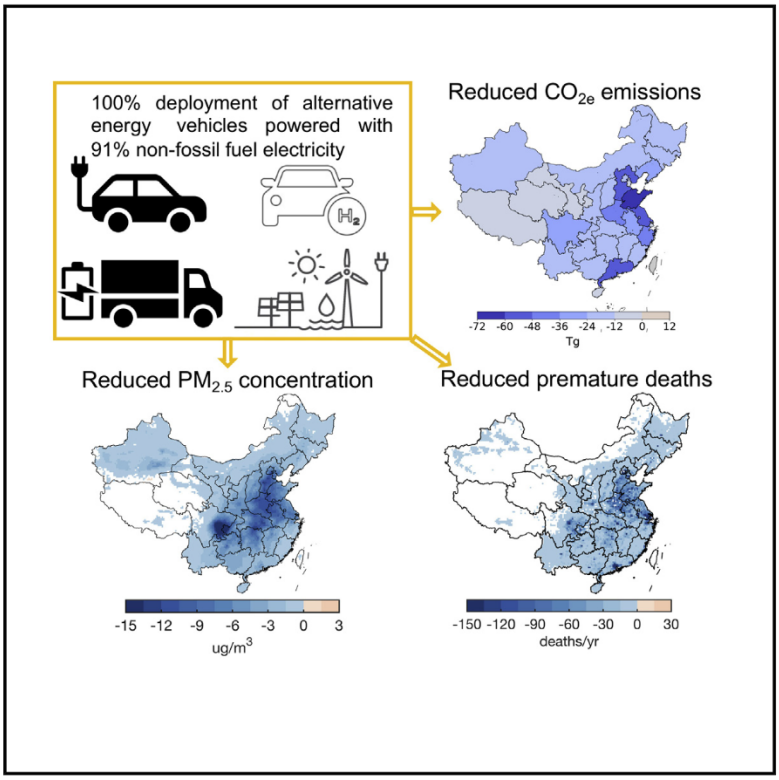

Authors

Liqun Peng, Feiqi Liu, Mi Zhou, Mingwei Li, Qiang Zhang, Denise L. Mauzerall

Correspondence

mauzerall@princeton.edu

In brief

We estimate the co-benefits of AEV utilization for air quality, health, and climate, and evaluate the economic benefits of AEV penetration with various levels of decarbonized electricity in China. We find that air quality and GHG mitigation co-benefits through alternative energy vehicle deployment increases as the power sector decarbonized. Co-benefits are maximized via high penetration of AEV deployment powered with ambitious and rapid power sector decarbonization.

Highlights

- Deployment of AEVs decreases vehicle tailpipe emissions
- Decarbonized power generation is critical to reduce upstream emissions
- Coupling AEV penetration with decarbonized electricity is critical for total benefits
- Large air quality, climate, health, and economic co-benefits can be obtained

Peng et al., 2021, One Earth *4*, 1127–1140
August 20, 2021
https://doi.org/10.1016/j.oneear.2021.07.007

CellPress

One Earth

Gold Standard for the Global Goals | 3 tons of CO_2 offset

CellPress

Article

Alternative-energy-vehicles deployment delivers climate, air quality, and health co-benefits when coupled with decarbonizing power generation in China

Liqun Peng,[1] Feiqi Liu,[1,2] Mi Zhou,[1,3] Mingwei Li,[1] Qiang Zhang,[4] and Denise L. Mauzerall[1,5,6,*]

[1]Princeton School of Public and International Affairs, Princeton University, Princeton, NJ 08544, USA

[2]State Key Laboratory of Automotive Safety and Energy, Tsinghua University, Beijing 100084, China

[3]Laboratory for Climate and Ocean-Atmosphere Studies, Department of Atmospheric and Oceanic Sciences, School of Physics, Peking University, Beijing 100871, China

[4]Ministry of Education Key Laboratory for Earth System Modeling, Department of Earth System Science, Tsinghua University, Beijing 100084, China

[5]Department of Civil and Environmental Engineering, Princeton University, Princeton, NJ 08544, USA

[6]Lead contact

*Correspondence: mauzerall@princeton.edu

https://doi.org/10.1016/j.oneear.2021.07.007

SCIENCE FOR SOCIETY Aggressive deployment of alternative energy vehicles (AEVs) (e.g., electric vehicles and hydrogen fuel cell vehicles) coupled with decarbonized electricity and hydrogen can greatly reduce both tailpipe and powerplant emissions of air pollutants and GHGs bringing significant air quality, health, and climate co-benefits. However, to maximize benefits, energy decarbonization is critical. Previous studies have not quantified climate, air quality, and health benefits of AEVs powered with deeply decarbonized power generation nor included trucks and motorcycles in addition to passenger vehicles. Here, we include all types of AEVs powered with varying levels of decarbonized electricity sources. We find that deployment of AEVs coupled with simultaneous decarbonization of power generation yields the largest benefits. Full deployment of both effectively eliminates both tailpipe and power plant air pollutant and CO_{2e} emissions, thus delivering enormous air quality, health, and climate co-benefits.

SUMMARY

China is the world's largest carbon emitter and suffers from severe air pollution, which results in approximately one million premature deaths/year. Alternative energy vehicles (AEVs) (electric, hydrogen fuel cell, and natural gas vehicles) can reduce carbon emissions and improve air quality. However, climate, air quality, and health benefits of AEVs powered with deeply decarbonized power generation are poorly quantified. Here, we quantitatively estimate the air quality, health, carbon emission, and economic benefits of replacing internal combustion engine vehicles with various AEVs. We find co-benefits increase dramatically as the electricity grid decarbonizes and hydrogen is produced from non-fossil fuels. Relative to 2015, a conversion to AEVs using largely non-fossil power can reduce air pollution and associated premature mortalities and years of life lost by ~329,000 persons/year and ~1,611,000 life years/year. Thus, maximizing climate, air quality, and health benefits of AEV deployment in China requires rapid decarbonization of the power system.

INTRODUCTION

To meet the goal of the Paris Agreement, to limit global warming to less than 2°C above pre-industrial temperatures, global CO_2 emissions must approach net zero around 2050 (IPCC, 2018). As the world's top carbon emitter, China has faced both domestic and international pressure to reduce CO_2 emissions. China now aims to peak CO_2 emissions by 2030 and achieve carbon neutrality by 2060. Rapid industrialization has resulted in extreme levels of air pollution and China has declared a "war on air pollution" to improve air quality and protect public health. About one million premature mortalities in China were attributed to ambient $PM_{2.5}$ and O_3 pollution in 2017.[1] The decarbonization of the on-road transport sector offers opportunities to simultaneously reduce emissions of air pollutants and greenhouse gases (GHGs) and obtain climate, air quality, and human health benefits.

China's rapid economic growth has led to a dramatic increase in vehicle numbers which are a growing source of air pollutant and CO_2 emissions. Vehicle ownership in China grew from ~172 million vehicles in 2015 to 260 million vehicles in 2020.[2] According to the Multi-resolution Emissions In China (MEIC)[3] inventory, in 2015 on-road vehicle emissions accounted for 23%, 27%, 18%, and 9% of national NO_x, VOC, CO, and CO_2 emissions, respectively. Although heavy-duty trucks (HDTs) only accounted for 2.4% of total vehicle numbers (Table S1), they contributed approximately half of on-road NO_x and $PM_{2.5}$ emissions and one-third of on-road CO_2 emissions in 2015. Conversely, although the stock of on-road light-duty passenger vehicles (LDPVs) (e.g., private cars, taxies) accounted for more than 50% of total vehicle numbers, their share of vehicle NO_x and $PM_{2.5}$ emissions are only 4% and 6%, while their emissions of CO_2 are ~30% of total vehicle fleet emissions.[3]

Starting in 2012, China made an ambitious commitment to develop five million new energy vehicles by 2020, including plug-in hybrid electric vehicles (PHEVs), battery electric vehicles (BEVs), and hydrogen fuel cell electric vehicles (HFCVs).[4] In addition, between 2011 and 2019, the development of both compressed natural gas and liquid natural gas (CNG/LNG) vehicles and CNG/LNG fueling stations increased rapidly. Four factors motivate China's policy promotion of clean energy vehicles: (1) mitigation of air pollutant emissions from the transport sector and associated health benefits, (2) decarbonization of the vehicle sector to facilitate achievement of peak CO_2 emissions before 2030 and carbon neutrality before 2060, (3) improved alternative energy vehicles (AEVs) will provide a competitive advantage to Chinese vehicle manufacturers and allow them to increase market share in the global transportation market, and (4) increased penetration of AEVs will increase domestic energy security by reducing national dependence on oil imports.

Many findings[5–12] demonstrate that replacing internal combustion engine vehicles (ICEVs) with EVs can effectively improve air quality and public health, while mitigating GHG emissions. However, the magnitude of these benefits depends on the level of electricity decarbonization and the efficiency of the chosen vehicles. Additional studies[13–15] estimate the life-cycle emissions from HFCVs. Schnell et al.[16] illustrate that the potential of electric vehicles (EVs) to ameliorate extreme air pollution events in winter is limited and that the air quality and climate co-benefits of EVs depend on the emissions from power generation. Most previous studies focus on target years 2025 or 2030, which does not allow time to deeply decarbonize the power sector and hydrogen supply. They also focus only on either EVs or HFCVs. China's EV market is growing fast with 1.1 million EV sales in 2019.[17] While EVs certainly have the edge in today's passenger vehicle market due to their lower price and increasingly available charging infrastructure, HFCVs likely have their place in the future of mobility particularly in medium-duty trucks (MDTs) and HDTs. HFCVs are good options for long-distance travel of heavy-duty vehicles because of their good energy efficiency, fast refueling, and their relatively high-density energy source compared with current batteries. Thus, we consider both EVs and HFCVs when examining AEV replacement of ICEVs to achieve climate, air quality, and health benefits.

Our study goes beyond previous work by including all types of AEVs (EVs, electric motorcycles [EMCs], HFCVs, and CNG/LNG vehicles powered by a variety of electricity sources; see Note S1 and Table S2). We provide a comprehensive examination of how to maximize potential co-benefits for climate, air quality, and health of increased penetration of all types of AEVs and the importance of decarbonizing the power system to maximize these co-benefits. We begin with scenario development of various AEV penetrations and power sector energy mixes in China (see "scenario design" in the experimental procedures). Scenarios are described in Table 1 with analysis focused on those in bold. We estimate the reduced air pollutant and equivalent CO_2 (CO_{2e}) emissions from replacing ICEVs with AEVs as well as the increased emissions from electricity generation and upstream emissions (see "estimating air pollutants and GHG emissions" in the experimental procedures). We then employ an atmospheric chemistry transport model (WRF-Chem v.3.6.1) to simulate improvements in annual average air quality and summer O_3 concentrations over China from deployment of these AEVs using a variety of energy sources (see experimental procedures, "air quality simulations"). Finally, we estimate the

Table 1. AEVscenarios

Cases	Transport sector	Electricity for AEVs
Base case[a]	2015 on-road transport[a]	2015 power mix (25%; 3%)[a]
LP-2015	low AEV penetration (2%–50%)	2015 power mix (25%; 3%)
LP-LR[a]	low AEV penetration (2%–50%)[a]	low renewable penetration (40%; 15%)[a]
LP-HR	low AEV penetration (2%–50%)	high renewable penetration (85%; 6%)
IP-2015	intermediate AEV penetration (5%–80%)	2015 power mix (25%; 3%)
IP-LR	intermediate AEV penetration (5%–80%)	low renewable penetration (40%; 15%)
IP-HR	intermediate AEV penetration (5%–80%)	high renewable penetration (85%; 6%)
HP-2015	high AEV penetration (9%–100%)	2015 power mix (25%; 3%)
HP-LP	high AEV penetration (9%–100%)	low renewable penetration (40%; 15%)
HP-HR[a]	high AEV penetration (9%–100%)[a]	high renewable penetration (85%; 6%)[a]
MP-HR[a]	maximum AEV penetration (50%–100%)[a]	high renewable penetration (85%; 6%)[a]

Details of the scenarios are provided in the experimental procedures and Tables S3–S5. The percentages in parentheses under "transport sector" indicate the penetration of various types of AEVs. The first number indicates the penetration of EVs for trucks, and the second number indicates the penetration of EVs for buses and taxis. The penetration of passenger vehicles falls within the range of these two numbers. For percentages under "electricity for AEVs," the first number represents the penetration of renewable energy for power generation, and the second indicates the penetration of nuclear power. In all renewable penetration scenarios, the emission factor for coal and gas power plants is adjusted to expected 2030 levels. For all scenarios, electricity utilized in other sectors continues to use 2015 emission factors.

[a]Scenarios for which we simulate air quality.

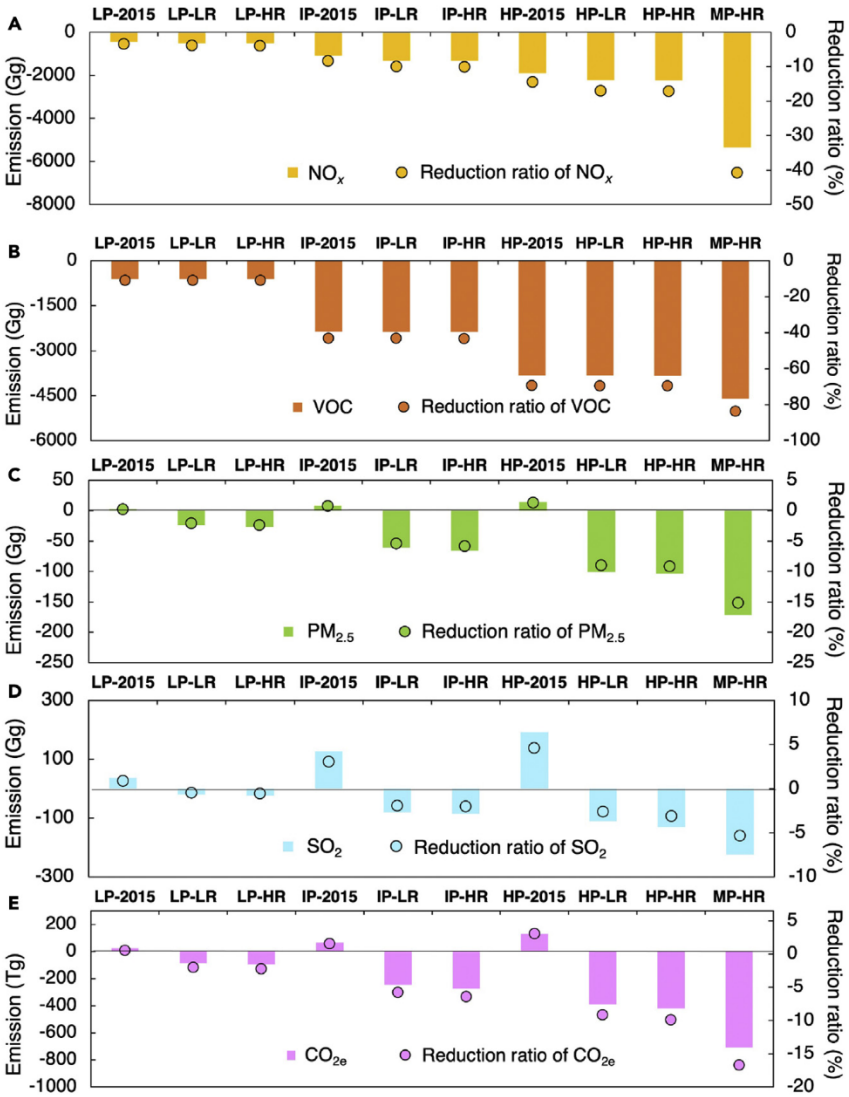

Figure 1. Changes in air pollutants and CO_{2e} emissions under each scenario

Changes in (A) NO_x, (B) VOC, (C) $PM_{2.5}$, (D) SO_2, and (E) CO_{2e} emissions from both vehicle tailpipes and energy sources for each scenario relative to the base case. Bars indicate the total emission changes compared with the base case. Dots indicate the percent reduction of emissions relative to the base case.

co-benefits of AEV utilization for air quality, health, and climate, and calculate the economic benefits of AEV penetration with various levels of electricity decarbonization in China (see experimental procedures). We find that climate, air quality, and human health co-benefits increase with increasing AEV penetration in the on-road transport sector with benefits increasing as electricity is increasingly decarbonized (at least 55% decarbonization is necessary to reduce emissions). In the most aggressive scenario (maximum penetration-high renewable [MP-HR]), in which we assume all vehicles are replaced by AEVs using a 91% non-fossil fuel penetration, annual population-weighted $PM_{2.5}$ and summer maximum daily 8 h average (MDA8) O_3 concentrations decrease by 5.7 $\mu g/m^3$ and 4.9 ppb, representing 9.1% and 7.8% reductions compared with the 2015 base case, respectively. Calculated avoided premature mortalities due to reduced exposure to ambient $PM_{2.5}$ and O_3 in the MP-HR scenario are 329,000 (95% confidence interval [CI]: 254,200–383,100). Our results illustrate the importance of simultaneously decarbonizing the power system while transforming the transport sector from ICEVs to AEVs.

RESULTS

Changes in total air pollutants and CO_{2e} emissions

Total air pollutants and CO_{2e} emissions will change as the penetration rate of AEVs and the level of grid decarbonization changes. Figure 1 shows the net change in total and percent of air pollutant emissions of NO_x, VOC, $PM_{2.5}$, SO_2, and CO_{2e} from vehicle tailpipes and energy sources for each scenario relative to the 2015 base case. Air pollutants (e.g., SO_2 and $PM_{2.5}$) and CO_{2e} emissions will increase if we increase the penetration of AEVs more rapidly than the electricity grid decarbonizes. We find the deployment of AEVs will result in reductions of all air pollutants and CO_{2e} emissions when the penetration of renewable power is above 40% (low renewable [LR] penetration scenario). Figure 2 separates the changes in emissions from vehicle tailpipes, the additional power generation required by the added AEVs, and upstream emissions from hydrogen and natural gas for each scenario. Emissions of all air pollutants and CO_{2e} decrease when AEV penetration and decarbonized power increase simultaneously. For all scenarios, the deployment of AEVs results in net reductions of NO_x and VOCs. However, in the 2015 power mix scenarios, which rely heavily on coal power, electrifying passenger vehicles and trucks increases total SO_2, $PM_{2.5}$, and carbon dioxide equivalent (CO_{2e}, GWP100) emissions (Figure 1; Table S7). When maximum penetration of AEVs is paired with high renewable electricity penetration (MP-HR scenario) the largest emission reductions are obtained. In the MP-HR scenario, emissions from vehicle tailpipes and the power sector together are reduced by ~41% of NO_x, 84% of VOC, 15% of $PM_{2.5}$, 5% of SO_2, and 17% of CO_{2e} of emissions in the 2015 base case. The provincial distribution of emission changes for each scenario is shown in Figures S1–S3.

Spatial distribution of air pollutant and CO_{2e} emissions

AEVs deployed in regions with clean electricity bring large emission reductions, while AEVs deployed in regions with dirty coal power result in increased emissions of air pollutants and CO_{2e}. In 2015, more than 85% of electricity in the north and northeast

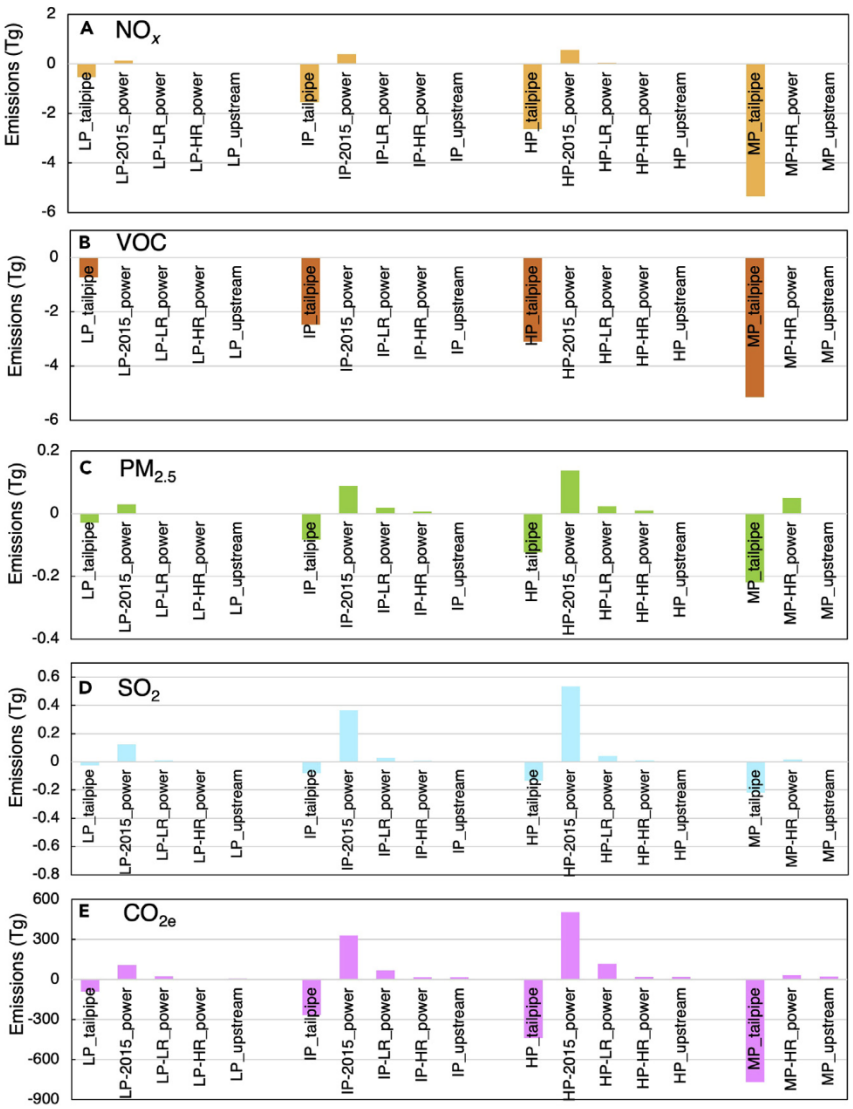

Figure 2. Changes in emissions from vehicle tailpipes, power generation, and upstream emissions from hydrogen and natural gas for each scenario

Emission changes of (A) NO_x, (B)VOC, (C) $PM_{2.5}$, (D) SO_2, and (E) CO_{2e}. For each pollutant we include emissions changes from conversion from the 2015 base case to each scenario. For each scenario we include (1) tailpipe emissions, (2) power generation emissions, and (3) upstream emissions from hydrogen production and leakage, leakage of natural gas during production, transport, and distribution. Scenarios include combinations of vehicle sector emissions (LP, IP, HP, and MP) powered by 2015, low- and high renewable penetration (LP and HR) electricity. Please see Table S6 for description of hydrogen production associated with each power scenario.

power grids came from coal-fired power plants.[18] Power grid details are shown in Figure S6. In 2015 the proportion of coal-fired electricity was between 60% and 70% in the northwest, east, and central grids.[18] The southern grid was the nation's cleanest regional grid and was the only one using less than 50% coal-fired electricity. Hydroelectricity is the largest source of power in the southern grid.

Figure 3A shows the change of air pollutant and CO_{2e} emissions when ICEVs are replaced with AEVs under the HP-2015 scenario compared with the 2015 base case. Although tailpipe emissions decrease, AEV deployment increases total SO_2 emissions for all provinces due to increased SO_2 emissions from the power sector that result. In addition, increases in $PM_{2.5}$ as well as CO_{2e} emissions occur in most provinces due to increased emissions from the 2015 power grid. However, high penetration (HP) of AEVs with the 2015 power mix still reduces NO_x and VOC emissions for all provinces, because the NO_x and VOC emissions from electricity needed for the AEVs is much less than their emissions from vehicles. Figure 3B shows the net change of air pollutant and CO_{2e} emissions when ICEVs are replaced with AEVs under the HP-HR scenario compared with the base case. In this scenario, AEV deployment significantly decreases emissions of NO_x, VOC, $PM_{2.5}$, and CO_{2e}, especially for the provinces with large vehicle populations and dirty electricity supply, such as Shandong, Jiangsu, and Guangdong, as decarbonized power replaces an additional 27% of coal power generation. Figure 3C shows the emission reductions attributable to decreases from the power sector when the 2015 power mix is replaced with 91% decarbonized electricity and hydrogen to AEVs. The differences of $PM_{2.5}$, SO_2, and CO_{2e} emissions between the 2015 power mix and 91% non-fossil grid are substantial, due to the high emission factors of $PM_{2.5}$, SO_2, and CO_{2e} for 2015 coal-fired power plants. Thus, a decarbonized power supply results in enormous air quality and CO_{2e} mitigation benefits from vehicles when AEVs are widely deployed.

Reductions in air pollutants and CO_{2e} tailpipe emissions

Tailpipe emissions dominate the emission reductions resulting from a replacement of ICEVs with AEVs. We analyze the change in tailpipe emissions that result across our four AEV scenarios. National tailpipe air pollutant emission reductions range from 10% to 100% for NO_x, 12%–100% for $PM_{2.5}$, 14%–100% for VOC, and 12%–100% for CO_{2e} across our scenarios (see Figure S7).

Replacing all ICEVs with AEVs (MP scenario) results in the largest reductions in primary $PM_{2.5}$, NO_x, VOC, and CO_2 tailpipe emissions. Emission reductions in the MP scenario (100%) are much higher than in the HP scenario (~50%–60%), because complete replacement of light-duty trucks (LDTs), MDTs, and HDTs with electric trucks and HFCVs occurs in the MP scenario. Replacement of trucks contributes more to air pollutant and CO_2 emission mitigation than replacing the LDPVs with AEVs, especially for NO_x and $PM_{2.5}$ emission reductions. This is because

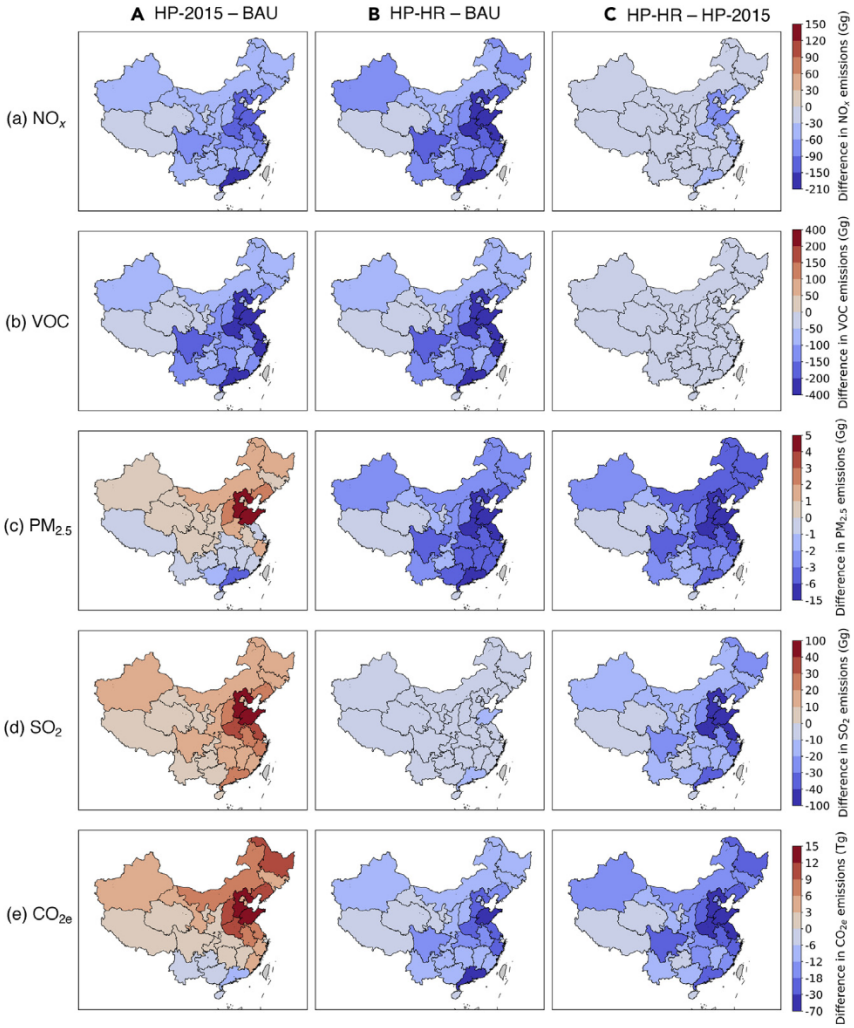

Figure 3. Comparison of provincial changes in air pollutants and CO_{2e} emissions from various AEV deployments and power sector decarbonization levels

Provincial changes in (A) NO_x, (B) VOC, (C) $PM_{2.5}$, (D) SO_2, and (E) CO_{2e} emissions under (A) HP-2015 scenario (high AEV penetration with 2015 power mix) compared with the base case (2015 on-road transport with 2015 power mix); (B) HP-HR scenario (high AEV penetration with high renewable penetration) compared with the base case; and (C) difference in air pollutants (A–D) and (E) CO_{2e} emissions between HP-HR scenario and HP-2015 scenario.

most trucks use diesel engines and both NO_x and $PM_{2.5}$ emission standards are weaker for diesel engines than gasoline engines.[19]

Total tailpipe emission reductions for each AEV technology type vary due to the extent of their uptake. Figure 4 shows the contribution of various AEV types to total on-road vehicle emission mitigation. Among AEVs, EVs and EMCs reduce emissions of all pollutants the most because EVs become the dominant type of AEV. For example, in Figure 4D, the MP scenario, 100% of private passenger vehicles, 100% of commercial passenger vehicles (e.g., buses and taxies), 100% of motorcycles, and 50% of trucks are electrified, while 50% of trucks are replaced with HFCVs. NO_x emission reductions from HFCVs are nearly as large as EVs and EMCs in the MP scenario, due to the large contribution of ICE trucks to NO_x emissions in the on-road transport sector.

Increases in air pollutants and CO_{2e} power sector and upstream emissions

The adoption of EVs and EMCs increase electricity demand and, in turn, increase electricity production and resulting air pollutant and CO_{2e} emissions. Depending on the decarbonization level of the power grid, this increased electricity demand offsets some of the benefits of tailpipe reductions from EVs. We estimate the increased electricity consumption from EVs in the transport sector based on the vehicle kilometers traveled (VKT) and electricity consumption per unit distance traveled (Figure S8). The increased electricity consumption is small compared with total electricity generation in China. For example, in the MP scenario, the increased electricity consumption is only 7% of total electricity generation in 2015 (NESY, 2016). In our four primary scenarios, private passenger vehicles dominate increases in electricity consumption because the electrification ratio of private passenger vehicles is higher than trucks and the stock of private passenger vehicles is much larger than commercial passenger vehicles. We compare the increased emissions from the electricity needed to charge EVs in various scenarios in Figure S9. We find that emissions increase when the 2015 power mix is used and increasingly decrease when 45% non-fossil and 91% non-fossil fuel power is used (see Figure 4). In this analysis, we neglect emissions associated with coal mining and hence may slightly underestimate emission reductions resulting from non-fossil electricity generation.

Since CO_{2e} emissions of hydrogen production from methane reforming is ~10 times higher than from electrolysis of water powered by renewable electricity.[20] We set up a sensitivity analysis that assumes 10%, 50%, 70%, and 90% of hydrogen production from renewable energy in low penetration (LP), intermediate penetration (IP), HP, and MP scenarios, respectively. Detailed descriptions of hydrogen source scenarios can be found in Table S6.

The adoption of natural gas vehicles (NGVs) and HFCVs increase the consumption of natural gas and hydrogen and further increase upstream emissions from the production and leakage of hydrogen and natural gas, which includes pre-production and gathering, processing, transmission, and storage, and distribution (Figure S10). However, the increased upstream emissions have only tiny impacts on emissions compared with the other

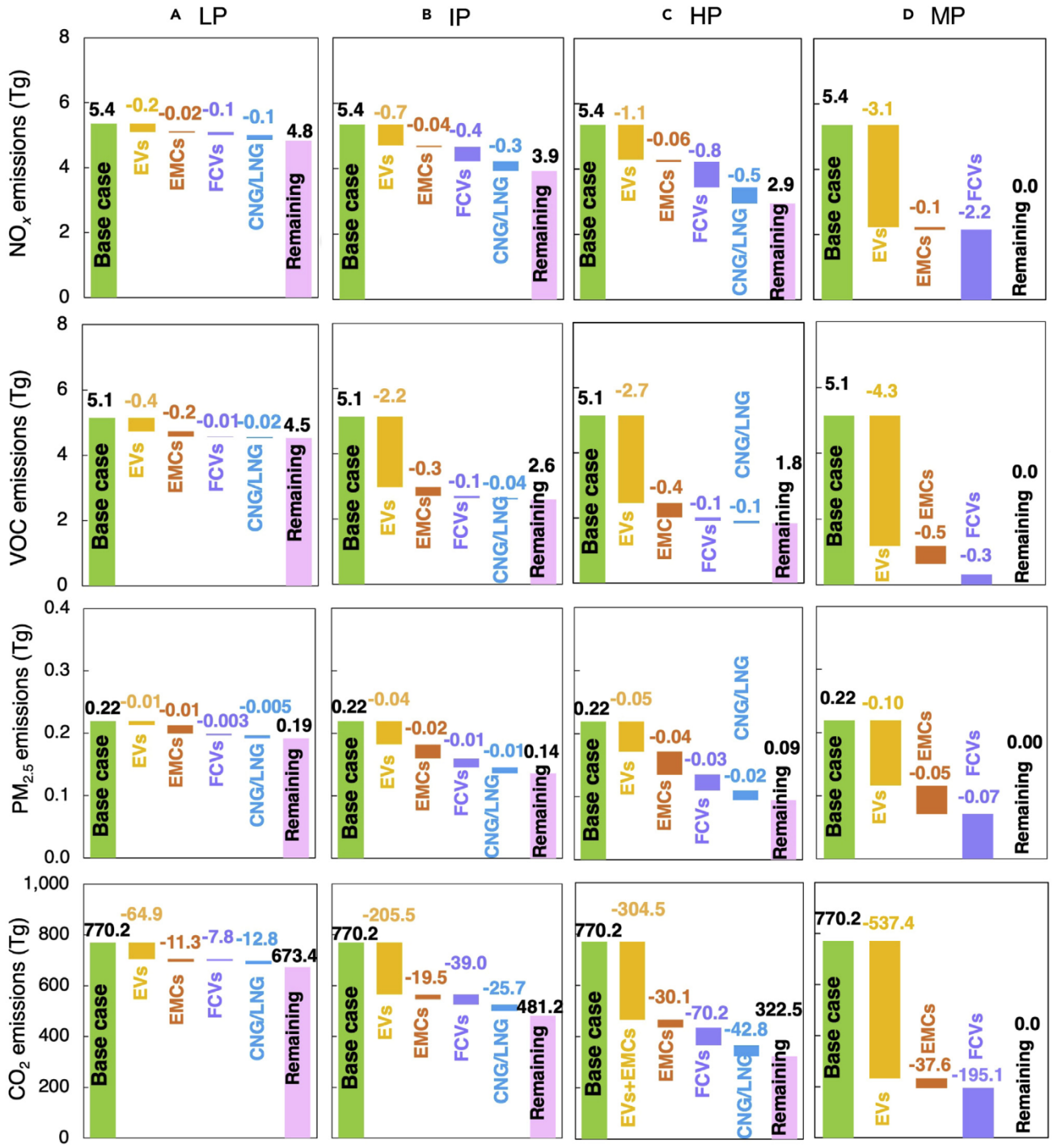

Figure 4. Contribution of EVs, EMCs, FCVs, and CNG/LNG vehicles to total reductions in tailpipe emissions from on-road vehicles

Yellow, purple, and blue bars and numbers indicate the reduced air pollutant and CO_{2e} emissions from EVs, EMCs, FCVs, and CNG/LNG vehicles under (A) low penetration (LP), (B) intermediate penetration (IP), (C) high penetration (HP), and (D) maximum penetration (MP) scenarios. The right pink bar in (A–D) represents the remaining tailpipe emissions from on-road vehicles. In the MP scenario (D), tailpipe emissions have been eliminated.

changes in the transport system, accounting for less than 0.03%–3% increase of the 2015 vehicle emissions by switching to NGVs and HFCVs. LDTs are the main contributor to upstream emissions from both hydrogen and natural gas, followed by HDTs and MDTs. LDTs and HDTs are responsible for almost 80% of total hydrogen and natural gas upstream emissions in all scenarios (Figure S10).

The absolute increase in $PM_{2.5}$ and CO_{2e} emissions from power generation and upstream natural gas and hydrogen production only account for 2%, 0.6%, and 0.6% and 0.1%, 0.2%, and

0.2% of net reductions in $PM_{2.5}$ and CO_{2e} emissions, respectively, from AEV deployment in LP-LR, HP-HR, and MP-HR scenarios, respectively. This indicates that, with HP of low-carbon electricity, using AEVs can greatly mitigate, and nearly eliminate, both air pollutant and CO_{2e} emissions.

Impacts on concentrations of surface air pollutants

We simulate China's 2015 base case surface air quality for January, May, July, and September using the WRF-Chem v.3.61 regional atmospheric chemistry transport model. We analyze reductions in NO_2, $PM_{2.5}$, and O_3 across China. Modeled $PM_{2.5}$ and ozone (O_3) concentrations are in good agreement with observations (Figures S13 and S14).

We find that replacement of ICEVs with AEVs in our scenarios will deliver an increasing reduction in annual average NO_2, $PM_{2.5}$, and O_3 concentrations nationwide (Figures 5 and S15) relative to the 2015 base case. The highest NO_2 reductions will occur in the most highly populated cities. The annual national population-weighted NO_2 reductions are 6.3 $\mu g/m^3$ in the MP-HR scenario due primarily to decreasing tailpipe emissions.

The air quality simulation results indicate that national annual average population-weighted $PM_{2.5}$ (from January and July simulations) would decrease by 0.6, 2.1, and 5.7 $\mu g/m^3$ in the LP-LR, HP-HR, and MP-HR scenarios, respectively, compared with the base case. The reduction of population-weighted $PM_{2.5}$ concentrations represents 1.0%, 3.4%, and 9.1% of base case $PM_{2.5}$ concentrations, respectively. The national annual average decreases in population-weighted $PM_{2.5}$ are largely from tailpipe emission reductions (Figure 2), suggesting that higher proportions of AEV penetration can readily lead to greater reductions in ambient $PM_{2.5}$ concentrations as long as the grid decarbonizes. The annual $PM_{2.5}$ reductions can reach 6.8 and 4.5 $\mu g\ m^{-3}$ in the MP-HR scenario in Beijing and Shanghai. These reductions are 5–8 times larger than the annual average $PM_{2.5}$ concentration reduction (0.8 $\mu g/m^3$) achieved nationally. This indicates that AEV deployment can result in significant air quality benefits in traffic-dense metropolitan urban areas. Our simulation results show that inorganic aerosols (nitrate, sulfate, and ammonium) account for 71% of $PM_{2.5}$ concentration reductions, with nitrate contributing 48% and sulfate contributing 7% (Figure S17A). Although NH_3 emissions remain constant, nitrate reduction contributes to lower ammonium aerosol concentrations.

Reductions in $PM_{2.5}$ concentrations have significant seasonal variations due to seasonally varying rates of secondary inorganic aerosol formation. Replacing ICEVs with AEVs decreases $PM_{2.5}$ concentrations in January more than in July (Figure S16) due to differences in temperature, humidity, and meteorology between summer and winter. For the MP-HR scenario, average population-weighted $PM_{2.5}$ concentrations decrease by 7.5 and 3.9 $\mu g/m^3$ in January and July, respectively. Based on our simulation results (Figures S17A and S17B), inorganic aerosol (nitrate, sulfate, and ammonium), BC and OC concentrations also decrease more in January than in July. Average population-weighted nitrate, sulfate, and ammonium concentrations decrease by 3.1, 0.5, and 1.1 $\mu g/m^3$ in January; 2.3, 0.3, and 0.8 $\mu g/m^3$ in July, respectively.

We find the adoption of AEVs results in widespread decreases of ground-level MDA8 O_3 concentrations in summer (May, July, and September simulations) in most areas of China due to the large resulting reductions in NO_x and VOCs. We find that summer MDA8 population-weighted O_3 concentrations over China decrease by 0.5, 2.8, and 4.9 ppb in the LP-LR, HP-HR, and MP-HR scenarios, respectively, representing 0.9%, 4.4%, and 7.8% reductions compared with the 2015 base case (Figure 5). The impacts on winter O_3 concentrations are more diverse (Figure S18), with slight decreases in regional O_3 concentrations and significant increases in most urban areas. Compared with the decreases in summer averages of MDA8 O_3, decreases in monthly averages of 24 h O_3 are smaller (Figure S19).

The change in monthly average 24 h O_3 is determined by whether the O_3 formation is in a VOC-limited or NO_x-limited regime. We use the ratio of the product of formaldehyde (HCHO) and hydrogen peroxide (H_2O_2) to nitrogen dioxide (NO_2) ($HCHO*H_2O_2/NO_2$) at the surface as a regime indicator, and use regime thresholds identified by Xing et al.[21] over East Asia (a ratio <1 being VOC limited and >1 being NO_x limited). Figure S20 shows that most areas in China are in a VOC-limited regime in winter, where O_3 increases when NO_x decreases. In comparison, the NO_x-limited areas, where O_3 decreases as NO_x decreases, are larger outside of winter. Although the North China Plain is in a VOC-limited regime, even in July, the simultaneous reduction of NO_x and VOC emissions in that area result in a monthly average decrease in 24 h O_3 in July as well.

Human health and economic benefits

We observe significant human health benefits of increased penetration of AEVs and increasing benefits as the power sector decarbonizes, primarily due to resulting reductions in annual ambient $PM_{2.5}$ and O_3 concentrations across China. We estimate that annually approximately 40,200 (95% CI: 30,000–63,000), 224,700 (95% CI: 187,400–279, 400), and 329,000 (95% CI: 254,200–383,100) premature deaths are avoided in LP-LR, HP-HR, and MP-HR scenarios due to reduced long-term exposure to annual $PM_{2.5}$ and O_3 concentrations. Gridded and provincial avoided premature mortalities in LP-LR, HP-HR, and MP-HR scenarios are shown in Figure S21 and Tables S11 and S12. The premature mortalities and years of life lost (YLL) attributed to ambient $PM_{2.5}$ and O_3 exposure in 2050 are shown in Tables S13–S16 by age group for the above three scenarios. Although total population changes little between 2015 and 2050, the population ages over those 35 years. The aging of the population results in larger numbers of premature mortalities and YLL by 2050 than if the age distribution had remained unchanged over that interval (see Tables S13–S20).

We further compare the monetary benefits of human health improvements and CO_{2e} emission reductions (Figure 6). A variety of methods are used to monetize air quality and climate benefits (see the experimental procedures). We estimate the economic benefits based on various baseline studies of value of statistical life (VSL)[22–27] and social cost of carbon (SCC).[28–32] The economic benefits of combining health benefits and GHG emission reductions due to ICEVs replacement with AEVs and increasing use of decarbonized power are US2015$6–187 billion, US2015$33–1102 billion, and US2015$49–1588 billion in LP-LR, HP-HR, and MP-HR scenarios, respectively. Between 2010 and 2018, average US VSL values ($18.9 million) were more than one order of magnitude higher than average Chinese VSL ($0.5 million)

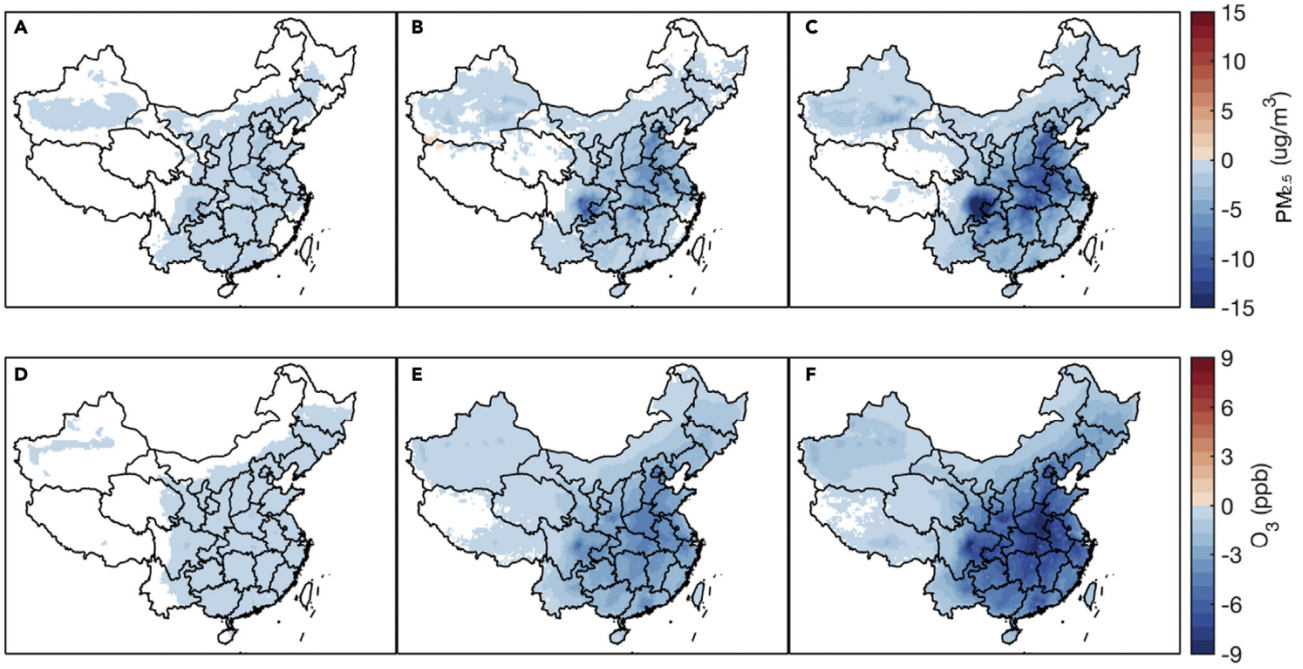

Figure 5. Reductions in simulated annual $PM_{2.5}$ and summer MDA8 O_3 concentrations

Reduced annual $PM_{2.5}$ concentrations from the (A) LP-LR, (B) HP-HR, and (C) MP-HR scenarios, respectively, compared with the base case. Reduced summer (May, July, and September) MDA8 O_3 concentration from the (D) LP-LR, (E) HP-HR, and (F) MP-HR scenarios, respectively, compared with the base case. See Figure S14 for MDA 8 O_3 concentration in January.

values. Despite relatively low VSL values for China, our results highlight enormous economic benefits of improving China's air quality and associated human health while mitigating GHG emissions by switching from traditional engine vehicles to AEVs across the country.

DISCUSSION

China is the largest emitter of CO_2 in the world. China's CO_2 emissions reached 10.2 Gt in 2019, accounting for 31% of global fossil fuel CO_2 emissions. To meet the Paris Agreement's target to limit global temperature increase to below 2°C above pre-industrial levels, net global CO_2 emissions must be carbon neutral by around mid-century.[33,34] In 2020, China pledged to reach net carbon neutrality by 2060. Carbon neutrality of the on-road transport sector is critical to achieve this goal. The rapid decarbonization of the electricity generated to power EVs is a critical component of achieving carbon neutrality of the transport sector as is the uptake of HFCVs using green hydrogen derived from non-fossil electricity to power HDTs. At the same time, China is suffering from severe air pollution due to rapid industrialization. Exposure to ambient air pollution is estimated to have resulted in one million premature mortalities in 2017.[1] Conversion of internal combustion engines to EV and HFC vehicles will eliminate tail pipe emissions of air pollutants and, if powered with renewable electricity, will also eliminate most air pollutant emissions from power generation. Despite the large opportunities from a transformation of the transport and power sector to non-fossil power, no prior systematic quantification of the benefits for GHG mitigation, air quality, and public health improvements of deep decarbonization has been made for China. Our study fills this gap by including passenger vehicles, motorcycles, HDTs, and the power sector (100% non-fossil energy for vehicles and 91% non-fossil energy for electricity and hydrogen).

We develop an integrated assessment framework to evaluate the implications of AEV penetration levels with various power system supply designs in China on GHG mitigation, air quality, and premature deaths. To evaluate the benefits of decarbonizing the transport sector, including both passenger vehicles, motorcycles, and trucks, and eliminate emissions of air pollutants, we simultaneously evaluate the adoption of various AEVs, suited for a variety of applications (e.g., EVs and EMCs as replacements for passenger cars and motorcycles, respectively, and HFCVs as a replacement for diesel trucks and buses) and consider the implications of a variety of energy sources for these AEVs. We find that increased AEV penetration alone increases $PM_{2.5}$, SO_2, and CO_{2e} emissions when AEVs are powered using electricity generated with the mix of technologies utilized in 2015 and hydrogen is derived from coal or natural gas rather than via water electrolysis using non-fossil electricity. We find that, for AEVs to yield air quality, health, and climate benefits, their uptake must be coupled with decarbonization of the power sector and the greater the level of decarbonization, the larger the benefits are for all three factors. For instance, if AEVs are powered primarily with fossil electricity (28% non-fossil energy), annual CO_{2e} emissions increase by 149 Tg. However, if AEVs are powered primarily with non-fossil energy (91% non-fossil energy), annual CO_{2e} emissions decrease by 420 Tg. Our findings indicate that simultaneously increasing uptake of AEVs while rapidly decarbonizing the power sector and hydrogen production, will yield the largest

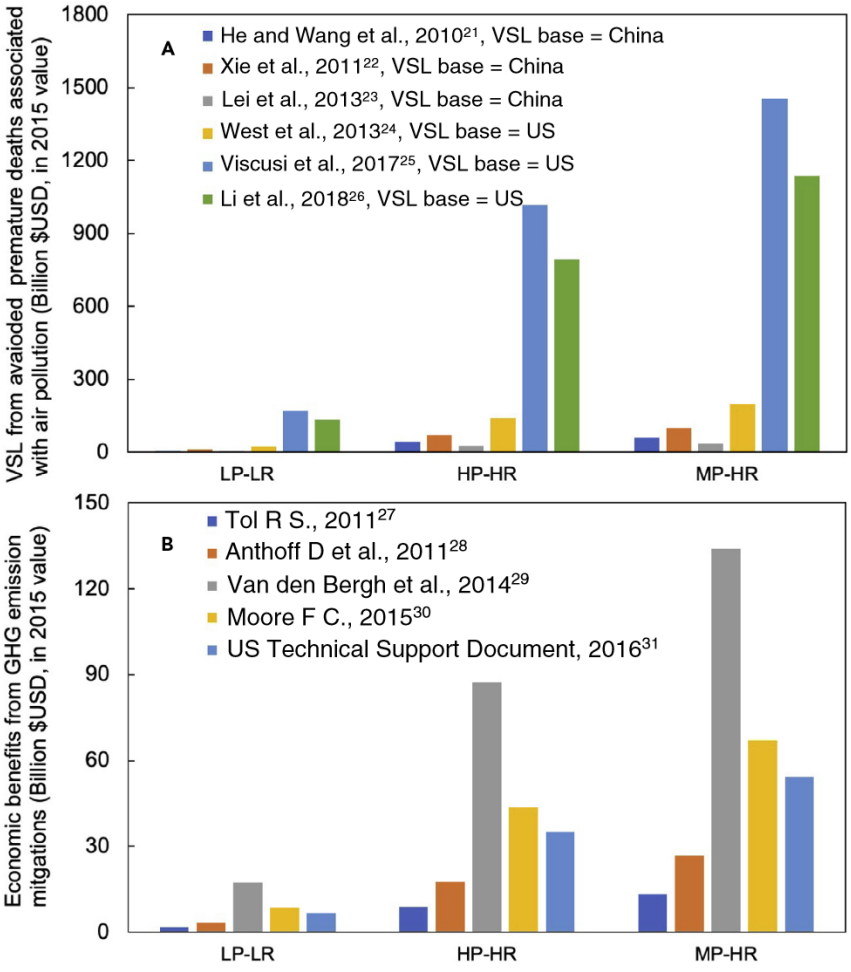

Figure 6. Comparison of economic benefits using valuations from various previous analyses

Data are shown for (A) VSL from avoided premature deaths and (B) economic benefits from reduced GHG emissions under LP-LR, HP-HR, and MP-HR scenarios, respectively. Colors indicate the data sources of VSL and SCC estimates.

co-benefits. Decarbonization of the power sector is of utmost importance in maximizing the benefits of increasing AEV penetration.

China's government recently announced a development plan for the new energy vehicle industry (EVs and HFCVs).[35] This plan states that, as of 2035, 50% of new cars sold in the country will be either electric, plug-in hybrid, or fuel cell vehicles, and 50% of new cars will be conventional hybrids, which still run entirely on gasoline but have improved fuel efficiency compared with ICEVs. Sales of new pure ICEVs (non-hybrid gas powered vehicles) will be banned starting in 2035. Although starting in 2021 EV adopters receive fewer monetary incentives than before, new supportive policy will focus on HFCVs to improve the industry's supply chain and technologies.[36] Municipal governments are now being encouraged to align environmental and industrial interests to incentivize AEV deployment in China. Current AEV policy puts China on a path for reduced air pollutant and carbon emissions from the vehicle sector as long as rapid decarbonization of power generation takes place simultaneously.

Currently, 67% of hydrogen production comes from fossil fuel (e.g., coal and natural gas), while the rest is a byproduct of industrial processes. Steam methane reforming dominates hydrogen production in China, accounting for 60% of total hydrogen production.[20] In comparison, water electrolysis using renewably generated electricity ("green hydrogen") only accounted for 3% of hydrogen production in 2020.[20] However, based on the White Paper on China's Hydrogen Energy and Fuel Cell Industry,[37] hydrogen production from renewable energy water electrolysis in 2050 will reach 70%, while the share of hydrogen from fossil fuel will drop to 20%. In our study, we set up a sensitivity analysis (Table S6) to estimate the potential emission mitigation from hydrogen production if non-fossil generated electricity with water electrolysis replaces fossil production of hydrogen. The results indicate that total air pollutant and CO_{2e} emissions from HFCVs would decrease by 73% if green hydrogen penetration increases from 10% to 90%.

To address the urgency of climate change and explore the potential of further improving air quality via AEV deployment, our study considered a variety of decarbonization levels for electricity generation and includes more AEV types than Liang et al.[11] or Schnell et al.[16] Liang et al.[11] estimated the air quality and health benefits of projected electric passenger vehicle penetration in 2030, given current policies, and found 17,456 (95% CI: 10,656–22,160) avoided annual premature deaths nationally due to reduced $PM_{2.5}$ and O_3 concentrations in China. We find that in our scenarios the avoided premature deaths due to an expansion of the AEV fleet including EVs, EMCs, HFCVs, and NGVs powered with over 90% decarbonized electricity could be as large as ~329,000 persons (95% CI: 254,200–383,100). Schnell et al.[16] found that the deployment of passenger and LDT EVs ameliorate several wintertime air pollution episodes, bring health benefits, and reduce CO_2 emissions when the marginal electricity generation is 50% emission-free. However, summer O_3 pollution is also detrimental to human health. Rather than analyzing air pollution episodes in a single season, we simulate changes in annual average air pollution levels for $PM_{2.5}$ and summer MDA8 O_3 concentrations as well as CO_2 emission reductions for each of our scenarios. We find summer MDA8 O_3 will decrease in all of our scenarios leading to a reduction in premature deaths of 31,300 (10% of the ~329,000 total avoided premature mortalities). A key difference between our work and both previous studies is that we consider higher penetration rates of AEVs powered with an 85% renewable electricity mix

(91% decarbonized power including nuclear) and in addition to EVs we also include EMCs, HFCVs, and NGVs. In our MP-HR scenario, NO_x, VOC, $PM_{2.5}$, SO_2, and CO_{2e} emissions from on-road vehicles only account for 0.3%, 1.2%, 1.1%, 7.0%, and 7.0% of the emissions of on-road vehicles in 2015. Our analysis also extends beyond previous studies to include changes in annual air pollution concentrations, resulting premature mortalities, and YLL. A conversion to AEVs using largely non-fossil power can reduce air pollution and associated YLL by ~ 1,611,000 life years per year compared with the 2015 base case.

Increased electricity demand will bring challenges and opportunities to the power grid system. In our study, we assume that the increased electricity demand for charging EVs is derived from newly built power plants. In addition, we assume that the power grid will be updated with increased power capacity, transmission, and distribution capacity, to support the increased demands resulting from AEV growth. However, future research on how to best meet the increased electricity demand while reducing emissions via incorporation of variable renewable generation, increased storage, and transmission is crucial.

Our results are subject to several uncertainties and limitations. First, we chose 2015 as the base year in this study as it was the most recent year for which we had access to complete data. Considering China's decreasing transport and power sector air pollutant emissions in recent years,[38] the environmental and health benefits in each scenario may be smaller than we estimated. Second, our scenarios are sensitivity analyses to investigate the implications of various AEVs powered with a variety of energy sources that the literature indicates are possible by 2050. However, because emissions from other sectors are kept at 2015 levels, these analyses do not represent actual 2050 air pollution concentrations, which may affect the health benefit estimates we made. Third, we did not include emissions from the off-road vehicle sector (e.g., agricultural machines and construction equipment). These emissions are substantial, and their elimination is needed to further improve air quality and achieve carbon neutrality. EV and HFCV technology could likely be used in these off-road applications. Future research on the co-benefits of replacing traditional agricultural and construction equipment with electric and hydrogen fuel cell engines is needed. Fourth, emissions from mining, transport, and distribution of fossil fuels used in the power sector, as well as emissions from the construction and disposal of power generation technology, are not included in our study.

In addition to the factors discussed above, the MEIC emission inventory we use assumes a perfect implementation of emission standards. However, due to limited inspection and maintenance in China MEIC underestimates actual air pollutant and CO_2 emissions from the transport sector.[39] We use MEIC to quantify the change of air pollutant (primary $PM_{2.5}$, NO_x, SO_2, VOC, BC, and OC), and CO_2 emissions resulting from various AEV scenarios. Anenberg et al.[39] show that actual NO_x emission factors for passenger cars, HDTs, and buses in China are 50%–330% higher than permitted by emission standards if they were perfectly enforced. Furthermore, MEIC was developed assuming that traffic volumes are homogeneous within provinces.[40] However, significant nonlocal truck traffic is not reflected in static registration data. Yang et al.[41] developed a link-level emission inventory based on multiple datasets extracted from the extensive road traffic-monitoring network in Beijing and argued that previous conventional emission inventories underestimated the emissions of both NO_x and $PM_{2.5}$ by ~45%, primarily due to missing contributions from nonlocal HDTs. As a result of these factors, our findings underestimate the benefits of conversion from ICEVs to AEVs.

In conclusion, we find that high AEV penetration must be coupled with deeply decarbonized electricity to maximize co-benefits for air quality, health, and GHG mitigation. If AEV penetration increases rapidly and is powered with the 2015 power mix (72% fossil fuel), $PM_{2.5}$, SO_2, and CO_{2e} emissions will increase. Decreasing fossil fuel used in the power sector to 45% (LR penetration scenario) decreases both air pollutant and CO_{2e} emissions from AEV deployment relative to the vehicle fleet emissions in 2015 (base case). High AEV penetration powered with 91% non-fossil fuel electricity (MP-HR, maximum penetration of AEVs with high renewable electricity scenario) maximizes air quality, health, and climate co-benefits. In this most aggressive scenario, national annual population-weighted $PM_{2.5}$, summer MDA8 O_3 concentrations, and CO_{2e} emissions decrease by 5.7 $\mu g/m^3$ (~9%), 4.9 ppb (~8%), and 708 Tg (~7%), respectively, of China's 2015 population-weighted concentrations and emissions. Calculated annual avoided premature mortalities and YLL due to reduced exposure to ambient $PM_{2.5}$ and O_3 in the MP-HR scenario are 329,000 (95% CI: 254,200–383,100) persons and ~1,611,000 (1,425,000–1,739, 200) YLL. Thus, we find that increased penetration of AEVs that use non-fossil generated electricity and hydrogen to replace highly polluting internal combustion engines will be a critical component of China's efforts to improve air quality while reaching net zero carbon emissions by 2060.

EXPERIMENTAL PROCEDURES

Resource availability

Lead contact

Further information and requests for data should be directed to the lead contact, Denise L. Mauzerall (mauzerall@princeton.edu).

Materials availability

This study did not generate new unique materials.

Data and code availability

The datasets and code generated during this study are available at https://doi.org/10.34770/2ye8-px32.

Scenario design

We set up various levels of AEV penetration and decarbonization levels for the power sector to present variability in the benefits resulting from future AEV penetration levels depending on possible penetration levels of various vehicle types and power sector electricity mixes (Figures S4 and S5) for 2050. The AEV penetration for passenger vehicles and trucks include LP, IP, HP, and an idealized MP scenario. The power generation mixes include LR and HR scenarios. The national total projections for LP, IP, and HP of AEVs in the transport sector, and LR and HR power generation scenarios are based on the uncertainty ranges of the 2050 projections by the Rocky Mountain Institute[42] (Reference Scenario and Reinventing Fire China Scenario, 2017) and the Chinese Energy Research Institute[43] (stated policies and below 2° scenario in the China Renewable Energy Outlook 2018). In the aggressive AEV scenario (MP scenario) we assume that 100% of ICEVs are replaced by AEVs.

The LP, IP, and HP scenarios describe the EV penetration ranges for passenger vehicles (7.5%–80%) and trucks (2%–9%), CNG/LNG penetration ranges for trucks (3%–6%), and hydrogen fuel cell vehicle penetration for trucks (2%–18%) from the literature.[42,43] Table S3 provides specific penetration rates for each type of alternative vehicle for each scenario and Table S4 provides scenarios of power generation mixes in 2050.

Estimating air pollutants and GHG emissions

We adopt a counterfactual method to evaluate the air quality, CO_2 mitigation, and health benefits of increasing penetration of AEVs with varying penetrations of decarbonized electricity. We use 2015 air pollutant emissions as our base case. For each scenario we keep all emissions outside the vehicle and power sectors the same as in our base case while changing emissions from the vehicle and power sectors. The changes reflect varying penetration rates of AEVs, as well as changes in emissions from the power sector for the electricity used to power the AEVs or generate hydrogen (e.g., reduced emission factors for coal and gas power plants, and two penetration levels for decarbonized electricity).

We use the bottom-up Multi-Resolution Emission Inventory of China (MEIC) developed by Tsinghua University in 2015 as our base case.[38] The MEIC inventory is a high-resolution anthropogenic air pollutant and carbon dioxide emission inventory for China. MEIC has a three-dimension matrix, which includes time, location, and emissions of each species (SO_2, NO_x, CO, NMVOC, NH_3, BC, OC, $PM_{2.5}$, PM_{10}, and CO_2). It includes ~800 anthropogenic sources, aggregated to five main sectors: power, industry, residential, transport, and agriculture. The emissions of a particular species are estimated by the following equation[44]:

$$E_i = \sum_j \sum_k A_{i,j,k} \left[\sum_m X_{i,j,k,m} EF_{j,k,m} (1 - \eta_n) \right]. \quad \text{(Equation 1)}$$

Here, i represents the province; j represents the sectors; k represents the fuel or product types; m represents the technology type for combustion and industrial process; n represents a specific control technology; A is the activity rate, such as fuel consumption; X is the fraction of fuel or production for a sector that is consumed by a specific technology; EF is the emission factor; η_n is the removal efficiency of control technology n.

We calculate both downstream emissions associated with end-use fuel (i.e., gasoline or diesel) combustion and upstream emissions associated with additional electricity generation, production, processing, transmission, and distribution of hydrogen and nature gas in each scenario.

We estimate the emission changes in a particular species of air pollutants and CO_2 emissions resulting from an AEV scenario in the transport sector as follows:

$$\Delta E_{i,T} = P_{i,j} \times E_{i,j}. \quad \text{(Equation 2)}$$

Here, ΔE represents change of emissions relative to the base case; T represents the transport sector; i represents province; P represents penetration of AEVs for each vehicle type j. Vehicle types include commercial passenger vehicles (including buses, taxies, and others), private passenger vehicles, trucks, and motorcycles. The proportion of BEVs and PHEVs in various vehicle fleets under LP, IP, HP, and MP scenarios is shown in Table S5 (see Note S2 for a more detailed description).

It is worth noting that there are no commercial vehicle emissions in MEIC. Commercial vehicle emissions are included in the passenger vehicle category. Therefore, we separate the emissions of buses and taxies from passenger vehicles in MEIC by using the 2015 population of buses and taxies,[45] 2015 VKT,[45] and emission factors.[46]

$$E_{i,CV} = Pop_{i,T} \times VKT_{i,T} \times EF_{i,T} + Pop_{i,B} \times VKT_{i,B} \times EF_{i,B}. \quad \text{(Equation 3)}$$

Here, E represents emissions of an air pollutant; i represents province; CV represents commercial vehicles; Pop represents the population of each vehicle type; VKT represents annual vehicle kilometers of each vehicle type; EF represent the emission factor; T and B represent taxies and bus vehicle types, respectively.

We estimate the emission changes in a particular species of air pollutants and CO_2 emissions in the power sector as follows:

$$\Delta E_{i,P} = Pop_{i,j} \times VKT_{i,j} \times ELE_{i,j} \times EF_{i,j}. \quad \text{(Equation 4)}$$

Here, ΔE is change of emissions of a pollutant from the power sector relative to the base case; P represents power sector; i and j represent provinces and vehicle types; Pop represents population of electrified vehicles for each vehicle type; VKT represents 2015 annual VKT (Table S8); ELE represents electricity consumption of electrified vehicles per kilometer (Table S8); and EF is the emission factor of air pollutants and CO_{2e} emissions from electricity generation used for the AEVs. Emission factors are derived from the existing literature (Table S9). We adopt the emission factors of coal and natural gas power plants in 2030 because we assume new power plants will be built to provide electricity for the new AEVs and that the emission control technologies for fossil fuel combustion by 2030 will be mature and will not decline significantly after 2030. We estimate annual VKT based on the average of lifetime vehicle miles traveled in typical cities in China in 2015.[47] Lifetime vehicle miles traveled is 165,000 km (102,525 mi) (assuming annual mileage of approximately 11,000 km [6,835 mi annual mileage], and a 15-year average vehicle lifetime [Ministry of Commerce of the People's Republic of China]).

We estimate annual upstream emissions from production, processing, transmission, and distribution of hydrogen and natural gas as follows:

$$E_{i,UP} = Pop_{i,n} \times VKT_{i,j,n} \times EF_{i,j,n} + Pop_{i,h} \times VKT_{i,j,h} \times EF_{i,j,h}. \quad \text{(Equation 5)}$$

Here, E is the increased emissions from natural gas and hydrogen; UP represents upstream emissions; i and j represent provinces and vehicle types; n and h represents natural gas and hydrogen fuel cell vehicles; Pop represents population of natural gas or hydrogen fuel cell vehicles; VKT represents annual VKT of natural gas or hydrogen fuel cell vehicles; EF represents the emission factor of air pollutants and CO_{2e} emissions from production, processing, transmission, and distribution of hydrogen or natural gas.[48–50]

Finally, we calculate the total emission changes in the transport and power sector for each scenario by using the same temporal and spatial distribution as MEIC 2015 and create monthly gridded emissions for each counterfactual scenario.

Air quality simulations

We simulate the ambient concentration changes of $PM_{2.5}$, O_3, and NO_2 for January, May, July, and September for the 2015 base case, LP-LR, HP-HR, and MP-HR scenarios using WRF-Chem v.3.6.1 (https://www2.acom.ucar.edu/wrf-chem). The model resolution is 27 × 27 km, and the domain covers China and parts of other Asian countries (9°N to 58°N and 60°E to 156°E). The model has 37 vertical layers from the surface (32 m) to 50 hPa. 2015 initial and lateral meteorological boundary conditions are provided by the National Centers for Environmental Prediction (NCEP) FNL (Final) Operational Global Analysis data (https://rda.ucar.edu/datasets/ds083.2/index.html) at 1° × 1° resolution. Chemical initial and boundary conditions are derived from the Community Atmosphere Model with Chemistry (CAM-Chem v.4).[51]

The physical and chemical schemes used in WRF-Chem are as follows: the RRTM scheme for longwave radiation,[52] the Goddard shortwave scheme,[53] the Morrison aerosol microphysics scheme,[54] the Noah land surface scheme,[55] the Yonsei University PBL scheme,[56] the model for simulating aerosol interactions and chemistry (MOSAIC) for aerosol,[57] and CBMZ[58] for gas-phase chemistry. Biogenic emissions are calculated online using the Model of Emission of Gases and Aerosols from Nature (MEGAN) coupled with WRF-Chem.[59] Natural dust emissions are calculated by the modified GOCART scheme.[60] We apply an improved scheme that better represents the formation of secondary inorganic aerosols.[61]

Because our simulations are only for 2015, we compare the meteorology during the winter (January) and summer (May, July, and September) of 2011, 2013, 2015, 2017, and 2019 with the average of 2011–2020 by using climate reanalysis data from the European Center for Medium-Range Weather Forecasts (https://www.ecmwf.int/). We find that, in January, May, July, and September of 2015, the mean boundary layer height is within 15%, the wind speed at 925 hPa is with 20% and the precipitation is within 50% of the 10-year average over most regions of China (Figures S11 and S12). We find that the meteorology for other years with which we compare diverges from the 10-year average by more than 2015, making us comfortable using 2015 for our analysis as others have done.[62,63] The modeled meteorological parameters (i.e., 2-m air temperature, dewpoint temperature, 10-m wind speed, and sea-level pressure) are compared with observations from the National Climate Data Center (Table S10). In Figures S13 and S14 we compare $PM_{2.5}$ dry mass concentrations and summer MDA8 O_3 concentrations in the base case with observations from the Ministry of Ecological Environment. We obtain good model agreement with observations across China in the months we simulate.

Analysis of health impacts associated with air pollution

We calculate the avoided premature mortalities attributed to the reduced ambient $PM_{2.5}$ and O_3 concentrations. Assessment of the ambient $PM_{2.5}$-associated premature mortality from noncommunicable diseases and lower respiratory infections (NCD + LRIs) is based on epidemiological cohort studies of long-term exposure to $PM_{2.5}$.[64] The reduction in premature deaths in each scenario is estimated as follows:

$$\Delta Mort_{i,p} = POP_{j,p} \times B_i \times \left(\frac{1}{RR_i(C_S)} - \frac{1}{RR_i(C_{BASE})}\right). \quad \text{(Equation 6)}$$

Here, $\Delta Mort_{i,p}$ is the change of premature mortality between base case and AEV scenarios in WRF-Chem grid p from disease i; $POP_{j,p}$ represents the number of population with age group j in grid p; B_i is the national base case mortality rate for each disease i; RR is the relative risk for disease i at the $PM_{2.5}$ concentration (C); Cs is the $PM_{2.5}$ concentration in various AEV scenarios; C_{BASE} is the $PM_{2.5}$ concentration in the base case. The RR for each disease is calculated from the exposure response function for a particular concentration of $PM_{2.5}$ based on the Global Exposure Mortality Model (GEMM).[64]

According to GEMM, relative risks (RR) of NCDs and LRIs associated with $PM_{2.5}$ exposure is calculated for adults (≥25 years old) using age groups with 5-year intervals from 25 to older than 85 years as follows:

$$RR(c) = e^{\frac{\theta * \log\left(\frac{c}{\alpha+1}\right)}{1+e^{\frac{c-\mu}{\nu}}}}, c = \max(0, c-2.4). \quad \text{(Equation 7)}$$

Here, c is long-term ambient $PM_{2.5}$ concentration; θ, σ, μ, and ν are parameters that determine the shape of RR in GEMM, and are specified for each age group. The values for σ, μ, and ν are constant across all age groups for NCD + LRI, while θ varies by age group. In our study, we perturb the value of θ based on its mean and standard error described in Burnett et al.[64] and generate 10,000 shapes of RR for each age interval. We further calculate the mean and 95% CIs of avoided premature deaths and potential YLL for each age interval in each AEV scenario.

Avoided premature deaths due to reduced ambient O_3 concentration are estimated as follows:

$$\Delta Mort_{i,p} = POP_{j,p} \times B_{i,p} \times \left(1 - \frac{1}{RR_i}\right). \quad \text{(Equation 8)}$$

We use a log-linear concentration-response function (CRF) between change in O_3 concentration and RR:

$$RR = \exp(-\beta \Delta c). \quad \text{(Equation 9)}$$

Here, $\Delta Mort_{i,p}$is the change in mortality attributable to long-term O_3 exposure; POP is the population of adults older than 30 years; Δc is the change in O_3 concentration between various AEV scenarios and the base case; β is the CRF slope calculated from a recent estimate of RR per 10 ppb increase in annual mean MDA8 O_3 of 1.02 (95% CI: 1.01–1.04) for all diseases.[65] We use the average MDA8 O_3 concentration for January, May, July, and September as the annual mean MDA8 O_3 concentration.

Age-specific mortality rates were calculated by dividing the number of deaths in each age group by the total deaths of all ages. The function for estimating YLL, which proposed by Romeder and McWhinnie[66] is as follows:

$$YLL = \sum_{i=1} (Age_{limit} - j - 0.5) * d_i. \quad \text{(Equation 10)}$$

Here, YLL is the summation of all age-specific YLLs; $Age_{limit}$is the upper limit of age, which we choose as 80 years based on the existing literature[67]; j is the mid-point of the class interval of each age group. For example, the mid-point of the class interval of 25–29 years is 27; 0.5 is a constant; d_i is the number of premature deaths due to $PM_{2.5}$ and O_3 exposure in each class interval.

Because our AEV scenarios were developed to reflect possible penetration rates by 2050, we project 2050 population to better represent the health benefits of each scenario. Gridded population in 2050 is derived by scaling gridded population data in 2015 from the Global Population for the World dataset,[68] based on population projections by country and by age group in 2050 from the United Nations World Population Prospects 2019 revision under a medium fertility scenario[69] assuming that the spatial distribution of population in each country in 2050 is the same as that in 2015. We find population changes between 2015 and 2050 are very slight but the age distribution is older, which will affect the number of premature mortalities and potential YLL due to exposure to air pollutants. Base case mortality rates for each disease are obtained from the Global Burden of Diseases study (http://ghdx.healthdata.org/). We assume base mortality rates are unchanged across the scenarios.

Evaluation of economic benefits of improved health and GHG mitigation

Monetizing air quality and climate benefits is controversial and is often based on the VSL (a measure of people's willingness to pay to reduce their mortality risk) and the SCC (the marginal global societal cost of emitting an additional ton of carbon), respectively. VSL estimates vary substantially across countries, age groups, and income groups.[70] Studies on the VSL have been widely conducted in the developed world, but few such studies can be found for developing countries. He and Wang,[22] Xie,[23] and Lei and Ho[24] have published VSL estimates from survey studies for China (low and high estimates $90,000 and $250,000). The baseline VSL based on the US is US$1.6 million (2005), US$9.6 million (2015), and US$7.7 million (2007) in West et al.,[25] Viscusi and Masterman,[26] and Li et al.[27] We estimate the air quality and climate benefits based on various baseline studies and present the results in Figure 6A. The VSL is estimated as follows:

$$VSL = VSL_{base} \times \left(\frac{pcGDP2015_{China}}{pcGDP_{Base}}\right)^{\eta}. \quad \text{(Equation 11)}$$

Here, VSL_{base} is the VSL in the year identified in the original manuscript; η is the income elasticity; and income elasticity is set to be 0.4 in this study.[71] $pcGDP2015_{China}$ and $pcGDP_{Base}$represent per capita GDP in 2015 for China and baseline GDP from the country of each study.

Most published estimates of the SCC have been derived from integrated assessment models that combine economic growth, climate processes, human health, policies, and feedbacks. Despite the inherent uncertainties in models such as these, they are the best tools currently available for estimating SCC. SCC estimates range from $20 to higher than $200/ton CO_2.[28–32] We estimate the uncertainty range of climate benefits based on these SCC estimates.

SUPPLEMENTAL INFORMATION

Supplemental information can be found online at https://doi.org/10.1016/j.oneear.2021.07.007.

ACKNOWLEDGMENTS

This work was funded by the Princeton School of Public and International Affairs, the Ma Huateng Foundation, the High Meadows Foundation, and the China Scholarship Council. We thank Daniel Horton for a constructive review of our manuscript.

AUTHOR CONTRIBUTIONS

L.P. and D.L.M. conceived the idea of this project and designed the research. L.P. estimated the emission reductions, simulated the air pollutant concentration changes, and calculated the health and economic benefits. F.L. contributed the carbon emissions of hydrogen fuel cell vehicles. M.Z. contributed to the WRF-Chem simulations. M.L. contributed to the estimations of health and economic benefits. Q.Z. provided the emissions of each type of vehicles by province. L.P. and D.L.M. wrote the manuscript. All authors discussed the results and commented on the manuscript.

DECLARATION OF INTERESTS

The authors declare no competing interests.

Received: January 18, 2021
Revised: May 10, 2021
Accepted: July 23, 2021
Published: August 20, 2021

REFERENCES

1. Yin, P., Brauer, M., Cohen, A.J., Wang, H., Li, J., Burnett, R.T., Stanaway, J.D., Causey, K., Larson, S., Godwin, W., et al. (2020). The effect of air pollution on deaths, disease burden, and life expectancy across China and its provinces, 1990–2017: an analysis for the Global Burden of Disease Study 2017. Lancet Planet. Health *4*, e386–e398.
2. Qiao, Q., and Lee, H. (2019). The role of electric vehicles in decarbonizing China's transportation sector. https://www.belfercenter.org/sites/default/files/files/publication/RoleEVsDecarbonizingChina.pdf.
3. (2019). MEIC, the Multi0resolution emissions in China. http://www.meicmodel.org/.
4. Millikin, M. (2012). China publishes plan to boost fuel-efficient and new energy vehicles and domestic auto industry; targeting 500K PHEVs and EVs in 2015, rising to 2M by 2020. Green. Car Congress.
5. Tessum, C.M., Hill, J.D., and Marshall, J. (2014). Life cycle air quality impacts of conventional and alternative light-duty transportation in the United States. Proc. Nat. Acad. Sci. U S A *111*, 18490–18495.
6. Huo, H., Cai, H., Zhang, Q., Liu, F., and He, K. (2015). Life-cycle assessment of greenhouse gas and air emissions of electric vehicles: a comparison between China and the U.S. Atmos. Environ. *108*, 107–116.
7. Tamayao, M.-A.M., Michalek, J.J., Hendrickson, C., and Azevedo, I.M.L. (2015). Regional variability and uncertainty of electric vehicle life cycle CO_2 emissions across the United States. Environ. Sci. Technol. *49*, 8844–8855.
8. Yuksel, T., Tamayao, M.-A.M., Hendrickson, C., Azevedo, I.M.L., and Michalek, J.J. (2016). Effect of regional grid mix, driving patterns and climate on the comparative carbon footprint of gasoline and plug-in electric vehicles in the United States. Environ. Res. Lett. *11*, 044007.
9. Peng, W., Yang, J., Lu, X., and Mauzerall, D.L. (2018). Potential co-benefits of electrification for air quality, health, and CO_2 mitigation in 2030 China. Appl. Energy *218*, 511–519.
10. Schnell, J.L., Naik, V., Horowitz, L.W., Paulot, F., Ginoux, P., Zhao, M., and Horton, D.E. (2019). Air quality impacts from the electrification of light-duty passenger vehicles in the United States. Atmos. Environ. *208*, 95–102.
11. Liang, X., Zhang, S., Wu, Y., Xing, J., He, X., Zhang, K.M., Wang, S., and Hao, J. (2019). Air quality and health benefits from fleet electrification in China. Nat. Sustain. *2*, 962–971.
12. Peters, D.R., Schnell, J.L., Kinney, P.L., Naik, V., and Horton, D.E. (2020). Public health and climate benefits and trade-offs of U.S. Vehicle electrification. GeoHealth *4*, e2020GH000275.
13. Granovskii, M., Dincer, I., and Rosen, M.A. (2006). Life cycle assessment of hydrogen fuel cell and gasoline vehicles. Int. J. Hydrogen Energy *31*, 337–352.
14. Hao, H., Mu, Z., Liu, Z., and Zhao, F. (2018). Abating transport GHG emissions by hydrogen fuel cell vehicles: chances for the developing world. Front. Energy *12*, 466–480.
15. Chen, Y., Hu, X., and Liu, J. (2019). Life cycle assessment of fuel cell vehicles considering the detailed vehicle components: comparison and scenario analysis in China based on different hydrogen production schemes. Energies *12*, 1–24.
16. Schnell, J.L., Peters, D.R., Wong, D.C., Lu, X., Guo, H., Zhang, H., Kinney, P.L., and Horton, D.E. (2021). Potential for electric vehicle adoption to mitigate extreme air quality events in China. Earth's Future *9*, e2020EF001788.
17. Global EV Outlook (2020). https://iea.blob.core.windows.net/assets/af46e012-18c2-44d6-becd-bad21fa844fd/Global_EV_Outlook_2020.pdf.
18. Shen, W., Han, W., Wallington, T.J., and Winkler, S.L. (2019). China electricity generation greenhouse gas emission intensity in 2030: implications for electric vehicles. Environ. Sci. Technol. *53*, 6063–6072.
19. Wu, Y., Zhang, S., Hao, J., Liu, H., Wu, X., Hu, J., Walsh, M.P., Wallington, T.J., Zhang, K.M., and Stevanovic, S. (2017). On-road vehicle emissions and their control in China: a review and outlook. Sci. Total Environ. *574*, 332–349.
20. Liu, F., Mauzerall, D.L., Zhao, F., and Hao, H. (2021). Deployment of fuel cell vehicles in China: greenhouse gas emission reductions from converting the heavy-duty truck fleet from diesel and natural gas to hydrogen. Int. J. Hydrogen Energy *46*, 17982–17997.
21. Xing, J., Ding, D., Wang, S., Dong, Z., Kelly, J.T., Jang, C., Zhu, Y., and Hao, J. (2019). Development and application of observable response indicators for design of an effective ozone and fine-particle pollution control strategy in China. Atmos. Chem. Phys. *19*, 13627–13646.
22. He, J., and Wang, H. (2010). The Value of Statistical Life: A Contingent Investigation in China (The World Bank).
23. Xie, X.. (2011). The value of health: method for environmental impact assessment and strategis for urban air pollution control.
24. Lei, Y., and Ho, M.S. (2013). The valuation of health damages. In Clearer Skies over China: Reconciling Air Quality, Climate, and Economic Goals (The MIT Press). https://doi.org/10.7551/mitpress/9780262019880.001.0001.
25. West, J.J., Smith, S.J., Silva, R.A., Naik, V., Zhang, Y., Adelman, Z., Fry, M.M., Anenberg, S., Horowitz, L.W., and Lamarque, J.-F. (2013). Co-benefits of mitigating global greenhouse gas emissions for future air quality and human health. Nat. Clim. Change *3*, 885–889.
26. Viscusi, W.K., and Masterman, C.J. (2017). Income elasticities and global values of a statistical life. J. Benefit Cost Anal *8*, 226–250.
27. Li, M., Zhang, D., Li, C.-T., Mulvaney, K.M., Selin, N.E., and Karplus, V.J. (2018). Air quality co-benefits of carbon pricing in China. Nat. Clim. Change *8*, 398–403.
28. Tol, R. (2011). The social cost of carbon. Annu. Rev. Resour. Econ. *3*, 419–443.
29. Anthoff, D., Rose, S., Tol, R.S.J., and Waldhoff, S.T. (2011). Regional and sectoral estimates of the social cost of carbon: an application of fund. SSRN J. http://www.economics-ejournal.org/economics/discussionpapers/2011-18.
30. van den Bergh, J.C.J.M., and Botzen, W.J.W. (2014). A lower bound to the social cost of CO_2 emissions. Nat. Clim. Change *4*, 253–258.
31. Moore, F.C., and Diaz, D.B. (2015). Temperature impacts on economic growth warrant stringent mitigation policy. Nat. Clim. Change *5*, 127–131.
32. Technical Support Document: Technical Update of the Social Cost of Carbon for Regulatory Impact Analysis Under Executive Order 12866 (Interagency Working Group on Social Cost of Greenhouse Gases, US Government, 2016).
33. Millar, R.J., Fuglestvedt, J.S., Friedlingstein, P., Rogelj, J., Grubb, M.J., Matthews, H.D., Skeie, R.B., Forster, P.M., Frame, D.J., and Allen, M.R. (2017). Emission budgets and pathways consistent with limiting warming to 1.5 °C. Nat. Geosci *10*, 741–747.
34. Tokarska, K.B., and Gillett, N.P. (2018). Cumulative carbon emissions budgets consistent with 1.5°C global warming. Nat. Clim. Change *8*, 296–299.
35. Office of the State Council. (2020). The development plan of new energy vehicle industry from 2021–2035. http://www.gov.cn/zhengce/content/2020-11/02/content_5556716.htm.
36. (2020). China's subsidies to fast-track development of fuel cell vehicles. https://asia.nikkei.com/Business/Automobiles/China-s-subsidies-to-fast-track-development-of-fuel-cell-vehicles.
37. China Hydrogen Alliance. White paper on China's hydrogen energy and fuel cell industry. (2019).
38. Zheng, B., Tong, D., Li, M., Liu, F., Hong, C., Geng, G., Li, H., Li, X., Peng, L., Qi, J., et al. (2018). Trends in China's anthropogenic emissions since 2010 as the consequence of clean air actions. Atmos. Chem. Phys. *18*, 14095–14111.
39. Anenberg, S.C., Miller, J., Minjares, R., Du, L., Henze, D.K., Lacey, F., Malley, C.S., Emberson, L., Franco, V., Klimont, Z., et al. (2017). Impacts and mitigation of excess diesel-related NO_x emissions in 11 major vehicle markets. Nature *545*, 467–471.
40. Li, M., Liu, H., Geng, G., Hong, C., Liu, F., Song, Y., Tong, D., Zheng, B., Cui, H., Man, H., et al. (2017). Anthropogenic emission inventories in China: a review. Natl. Sci. Rev. *4*, 834–866.

41. Yang, D., Zhang, S., Niu, T., Wang, Y., Xu, H., Zhang, K.M., and Wu, Y. (2019). High-resolution mapping of vehicle emissions of atmospheric pollutants based on large-scale, real-world traffic datasets. Atmos. Chem. Phys. *19*, 8831–8843.

42. Energy Research Institute, Lawrence Berkeley National Laboratory and Rocky Mountain Institue (2019). Reinventing Fire: China. A roadmap for China's Revolution in Energy Consumption and Production to 2050, https://rmi.org/insight/reinventing-fire-china/.

43. China National Renewable Energy Centre (2018). China Renewable Energy Outlook 2018. https://resources.solarbusinesshub.com/solar-industry-reports/item/china-renewable-energy-outlook-2018-creo-2018.

44. Zhang, Q., Streets, D.G., Carmichael, G.R., He, K.B., Huo, H., Kannari, A., Klimont, Z., Park, I.S., Reddy, S., Fu, J.S., et al. (2009). Asian emissions in 2006 for the NASA INTEX-B mission. Atmos. Chem. Phys. *9*, 5131–5153.

45. Chen, X., Zhang, H., Xu, Z., Nielsen, C.P., McElroy, M.B., and Lv, J. (2018). Impacts of fleet types and charging modes for electric vehicles on emissions under different penetrations of wind power. Nat. Energy *3*, 413–421.

46. Zhang, S., Niu, T., Wu, Y., Zhang, K.M., Wallington, T.J., Xie, Q., Wu, X., and Xu, H. (2018). Fine-grained vehicle emission management using intelligent transportation system data. Environ. Pollut. *241*, 1027–1037.

47. Innovation Center for Energy and Transportation. (2018). 2018 new data analysis on real-world driving and fuel consumption for passenger cars in China. https://cdn.xiaoxiongyouhao.com/partner/icet/icet_xxyh_2018.pdf.

48. Tong, F., Jaramillo, P., and Azevedo, I.M.L. (2015). Comparison of life cycle greenhouse gases from natural gas pathways for medium and heavy-duty vehicles. Environ. Sci. Technol. *49*, 7123–7133.

49. Qin, Y., Höglund-Isaksson, L., Byers, E., Feng, K., Wagner, F., Peng, W., and Mauzerall, D.L. (2018). Air quality-carbon-water synergies and trade-offs in China's natural gas industry. Nat. Sustain. *1*, 505.

50. Guo, Y., Tian, J., and Chen, L. (2020). Managing energy infrastructure to decarbonize industrial parks in China. Nat. Commun. *11*, 981.

51. Lamarque, J.-F., Emmons, L.K., Hess, P.G., Kinnison, D.E., Tilmes, S., Vitt, F., Heald, C.L., Holland, E.A., Lauritzen, P.H., Neu, J., et al. (2012). CAM-chem: description and evaluation of interactive atmospheric chemistry in the Community Earth System Model. Geosci. Model Dev. *5*, 369–411.

52. Mlawer, E.J., Taubman, S.J., Brown, P.D., Iacono, M.J., and Clough, S.A. (1997). Radiative transfer for inhomogeneous atmospheres: RRTM, a validated correlated-k model for the longwave. J. Geophys. Res. Atmosphere *102*, 16663–16682.

53. Chou, M.-D., and Suarez, M.J.. (1994). An efficient thermal infrared radiation parameterization for use in general circulation models. https://citeseerx.ist.psu.edu/viewdoc/download?doi=10.1.1.26.4850&rep=rep1&type=pdf.

54. Morrison, H., and Pinto, J.O. (2005). Mesoscale modeling of springtime arctic mixed-phase stratiform clouds using a new two-moment bulk microphysics scheme. J. Atmos. Sci. *62*, 3683–3704.

55. Chen, F., and Dudhia, J. (2001). Coupling an advanced land surface-hydrology model with the Penn State-NCAR MM5 modeling system. Part I: model implementation and sensitivity. Mon. Wea. Rev. *129*, 569–585.

56. Hong, S.-Y., Noh, Y., and Dudhia, J. (2006). A new vertical diffusion package with an explicit treatment of entrainment processes. Mon. Wea. Rev. *134*, 2318–2341.

57. Zaveri, R.A., Easter, R.C., Fast, J.D., and Peters, L.K. (2008). Model for simulating aerosol interactions and chemistry (MOSAIC). J. Geophys. Res. Atmosphere *113*, Art. No. D13204 113.

58. Zaveri, R.A., and Peters, L.K. (1999). A new lumped structure photochemical mechanism for large-scale applications. J. Geophys. Res. *104*, 30.

59. Guenther, A., Karl, T., Harley, P., Wiedinmyer, C., Palmer, P.I., and Geron, C. (2006). Estimates of global terrestrial isoprene emissions using MEGAN (model of emissions of gases and aerosols from nature). Atmos. Chem. Phys. *30*, 3181–3210. https://doi.org/10.5194/acp-6-3181-2006.

60. Jones, S.L., Adams-Selin, R., Hunt, E.D., Creighton, G.A., and Cetola, J.D. (2012). Update on modifications to WRF-CHEM GOCART for fine-scale dust forecasting at AFWA. AGU Fall Meeting Abstracts *33*, A33D–A0188.

61. Chen, D., Liu, Z., Fast, J., and Ban, J. (2016). Simulations of sulfate-nitrate-ammonium (SNA) aerosols during the extreme haze events over northern China in October 2014. Atmos. Chem. Phys. *16*, 10707–10724.

62. Xing, J., Lu, X., Wang, S., Wang, T., Ding, D., Yu, S., Shindell, D., Ou, Y., Morawska, L., Li, S., et al. (2020). The quest for improved air quality may push China to continue its CO_2 reduction beyond the Paris Commitment. PNAS *117*, 29535–29542.

63. Liu, M., Huang, X., Song, Y., Tang, J., Cao, J., Zhang, X., Zhang, Q., Wang, S., Xu, T., Kang, L., et al. Ammonia emission control in China would mitigate haze pollution and nitrogen deposition, but worsen acid rain. 6 Proc. Natl. Acad. Sci. U S A 116(16):7760-7765.

64. Burnett, R., Chen, H., Szyszkowicz, M., Fann, N., Hubbell, B., Pope, C.A., Apte, J.S., Brauer, M., Cohen, A., Weichenthal, S., et al. (2018). Global estimates of mortality associated with long-term exposure to outdoor fine particulate matter. PNAS *115*, 9592–9597.

65. Turner, M.C., Jerrett, M., Pope, C.A., 3rd, Krewski, D., Gapstur, S.M., Diver, W.R., Beckerman, B.S., Marshall, J.D., Su, J., Crouse, D.L., et al. (2016). Long-term ozone exposure and mortality in a large prospective study. Am. J. Respir. Crit. Care Med. *193*, 1134–1142.

66. Romeder, J.M., and McWhinnie, J.R. (1977). Potential years of life lost between ages 1 and 70: an indicator of premature mortality for health planning. Int. J. Epidemiol. *6*, 143–151.

67. Life expectancy at birth, total (years). United Nations World Population Prospects. https://data.worldbank.org/indicator/SP.DYN.LE00.IN?view=chart.

68. Center for International Earth Science Information Network - CIESIN Columbia University, Gridded Population of the World, Version 4 (GPWv4): Population Count Adjusted to Match 2015 Revision of UN WPP Country Totals. (2016). https://sedac.ciesin.columbia.edu/data/collection/gpw-v4/documentation.

69. United Nations Department of Economic and Social Affairs Population Division. (2019). World population prospects: the 2019 revision. https://esa.un.org/unpd/wpp/Download/Standard/Population/.

70. Viscusi, W.K., and Aldy, J.E. (2003). The value of a statistical life: a critical review of market estimates throughout the world. J. Risk Uncertain. *27*, 5–76.

71. Hammitt, J.K., and Robinson, L.A. (2011). The income elasticity of the value per statistical life: transferring estimates between high and low income populations. J. Benefit Cost Anal. *2*, 1–29.